CNN-Based Flow Control Device Modelling On Aerodynamic Airfoils

Koldo Portal-Porras
University of the Basque Country
Unai Fernandez-Gamiz (unai.fernandez@ehu.eus)
University of the Basque Country
Ekaitz Zulueta
University of the Basque Country
Alejandro Ballesteros-Coll
University of the Basque Country
Asier Zulueta
University of the Basque Country

Research Article

Keywords: Computational Fluid Dynamics, CFD, Deep Learning, Convolutional Neural Network, CNN, airfoil, flow control devices, cell-set model

Posted Date: November 5th, 2021

DOI: https://doi.org/10.21203/rs.3.rs-1019389/v1

CNN-based Flow Control Device Modelling on Aerodynamic Airfoils

Koldo Portal-Porras [1], Unai Fernandez-Gamiz [1,*] , Ekaitz Zulueta [2], Alejandro Ballesteros-Coll [1] and Asier Zulueta [1]

[1] Nuclear Engineering and Fluid Mechanics Department, University of the Basque Country, UPV/EHU, Nieves Cano 12, Vitoria-Gasteiz, 01006 Araba, Spain; koldo.portal@ehu.eus (K.P.-P.); aballesteros013@ehu.eus (A.B.-C.); azulueta@arrasate.eus (A.Z.)

[2] System Engineering and Automation Control Department, University of the Basque Country, UPV/EHU, Nieves Cano 12, Vitoria-Gasteiz, 01006 Araba, Spain; ekaitz.zulueta@ehu.eus (E.Z.)

* Correspondence: unai.fernandez@ehu.eus

Abstract: Wind energy has become an important source of electricity generation, with the aim of achieving a cleaner and more sustainable energy model. However, wind turbine performance improvement is required to compete with conventional energy resources. To achieve this improvement, flow control devices are implemented on airfoils. Computational Fluid Dynamics (CFD) simulations are the most popular method for analyzing this kind of devices, but in recent years, with the growth of Artificial Intelligence, predicting flow characteristics using neural networks is becoming increasingly popular.

In this work, 158 different CFD simulations of a DU91W(2)250 airfoil are conducted, with two different flow control devices, rotating microtabs and Gurney flaps, added on its Trailing Edge (TE). These flow control devices are implemented by using the cell-set meshing technique. These simulations are used to train and test a Convolutional Neural Network (CNN) for velocity and pressure field prediction and another CNN for aerodynamic coefficient prediction. The results show that the proposed CNN for field prediction is able to accurately predict the main characteristics of the flow around the flow control device, showing very slight errors. Regarding the aerodynamic coefficients, the proposed CNN is also capable to predict them reliably, being able to properly predict both the trend and the values. In comparison with CFD simulations, the use of the CNNs reduces the computational time in four orders of magnitude.

Keywords: Computational Fluid Dynamics; CFD; Deep Learning; Convolutional Neural Network; CNN; airfoil; flow control devices; cell-set model

1. Introduction

In recent years, with the aim of achieving a cleaner and more sustainable energy model, wind energy has become an important source of electricity generation. Even so, an improvement in wind turbine performance is still required in order to compete with conventional energy sources in terms of energy production and associated costs. To solve this challenge, there are several solutions, for example, Barlas and van Kuik [1] reviewed the available advanced control concepts to reduce loads on the rotor. Another widely used solution is the implementation of both active, such as rotating microtabs, and passive, such as Gurney flaps, flow control devices. Aramendia et al. [2,3] extensively reviewed the available active and passive flow control devices for wind turbines.

There are experimental studies in which these devices are analyzed, such as the study of Alber et al. [4] for Gurney flaps and the one of Nakafuji et al. [5] for microtabs, but simulations by means of CFD tools are the most popular method for analyzing and optimizing the performance of airfoils and their flow control devices. Many authors have studied several different flow control devices applied on airfoils by means of CFD. For example, Fernandez-Gamiz et al. [6] and Aramendia et al. [7] performed parametric studies to analyze the effects of the implementation of passive microtabs and Gurney flaps, respectively, on the TE of the DU91W(2)250 airfoil.

In some cases, CFD simulations can be very demanding in terms of computational time and resources, especially when several simulations are necessary to optimize a flow control device or accurate turbulence modeling is required. For this reason, many authors have used alternative meshing models to reduce simulation time. Among these models, the cell-set model, introduced by Ballesteros-Coll et al. [8] can be highlighted. In that work, different Gurney flaps were added to the TE of a DU91W(2)250 airfoil by means of the cell-set model. In further studies, Ballesteros-Coll et al. [9] implemented rotating microtabs on the same airfoil. Other authors, such as Portal-Porras et al. [10,11] used this meshing technique to model the performance of three-dimensional Vortex Generators (VG) on a flat plate. All of them showed good agreements between the cell-set model, the fully-resolved model and the experimental data. Therefore, this meshing model is considered suitable for this kind of problems.

Despite the accurate predictions that can be obtained through CFD simulations, the increase in the computing speed of computers and the growth of Artificial Intelligence (AI) have led to an

increasing number of studies in which Deep Learning (DL) techniques are used for flow prediction, obtaining a significant reduction in terms of computing time. For example, Ye et al. [12] proposed a Convolutional Neural Network (CNN) to predict the pressure distributions around a cylinder based on the velocity field on its wake behind, Guo et al. [13] and Ribeiro et al. [14] designed different CNNs for two- and three-dimensional laminar flow prediction, Portal-Porras et al. [15] used a CNN to predict turbulent flows on a channel, and Abucide-Armas et al. [16] proposed a data augmentation technique to improve the predictions of the CNN proposed by Ribeiro et al. [14] for unsteady turbulent flows.

Regarding airfoils and their flow control devices, Thuerey et al. [17] proposed a CNN to approximate the velocity and pressure fields obtained by Reynolds-Averaged Navier-Stokes (RANS)-based Spalart-Allmaras [18] turbulence model on airfoils, and Bhatnagar et al. [19] created a CNN to predict flow fields around airfoils. Chen et al. [20] used a CNN to predict the drag (C_D) and lift (C_L) coefficients of different airfoils, and Rodriguez-Eguila et al. [21] modelled the lift-to-drag ratio (C_L/C_D) of three different airfoils with flaps on their TE by means of an Artificial Neural Network (ANN).

The present paper aims to predict the velocity and pressure fields around different Gurney flaps and rotating microtabs implemented on the TE of the DU91W(2)250 airfoil by means of a CNN. In addition, a variation of the CNN is proposed to predict the C_D and C_L coefficients of the studied airfoil with each flow control device.

The remainder of the manuscript is structured as follows: Section 2 provides an explanation of the methodology followed for preparing and running the CFD simulations and designing and training the proposed CNNs; Section 3 shows qualitative and quantitative comparisons between the CFD results and CNN predictions; and Section 4 explains the conclusions reached from this study.

2. Methodology

2.1. CFD Setup

With the purpose of obtaining data for training, validating and testing the proposed neural network, 158 CFD simulations of the DU91W(2)250 airfoil were conducted, each one under different conditions in terms of flow control device geometry and angle of attack (AoA). The selected profile, DU91W(2)250, is a profile extracted from a broadly referenced NREL horizontal axis wind

turbine (HAWT), as stated by Jonkman et al. [22]. Star-CCM+ v2019.1 [23] commercial code was used to run these simulations.

To perform the mentioned simulations, a two-dimensional structured O-mesh was generated, with the studied airfoil on its center. Following the study of Sørensen et al. [24], the radius of this mesh (R) was defined as a function of the chord length (c) of the airfoil, $R = 32 \cdot c$. Therefore, as the chord length of the DU91W250 airfoil is equal to 1 m, R was set at 32 m. This mesh consists of around 207,000 cells. Non-slip conditions were assigned to the contour of the airfoil, and the first cell height (Δz) normalized with the chord length of the airfoil was set at $\Delta z/c = 1.35 \cdot 10^{-6}$. On previous works, Fernandez-Gamiz et al. [6] studied the mesh dependency of the used mesh, and showed a dependency below 4% for the calculation of C_L and drag C_D coefficients. Figure 1a provides a general view of the mesh, and Figure 1b a close-up view of the near-airfoil region.

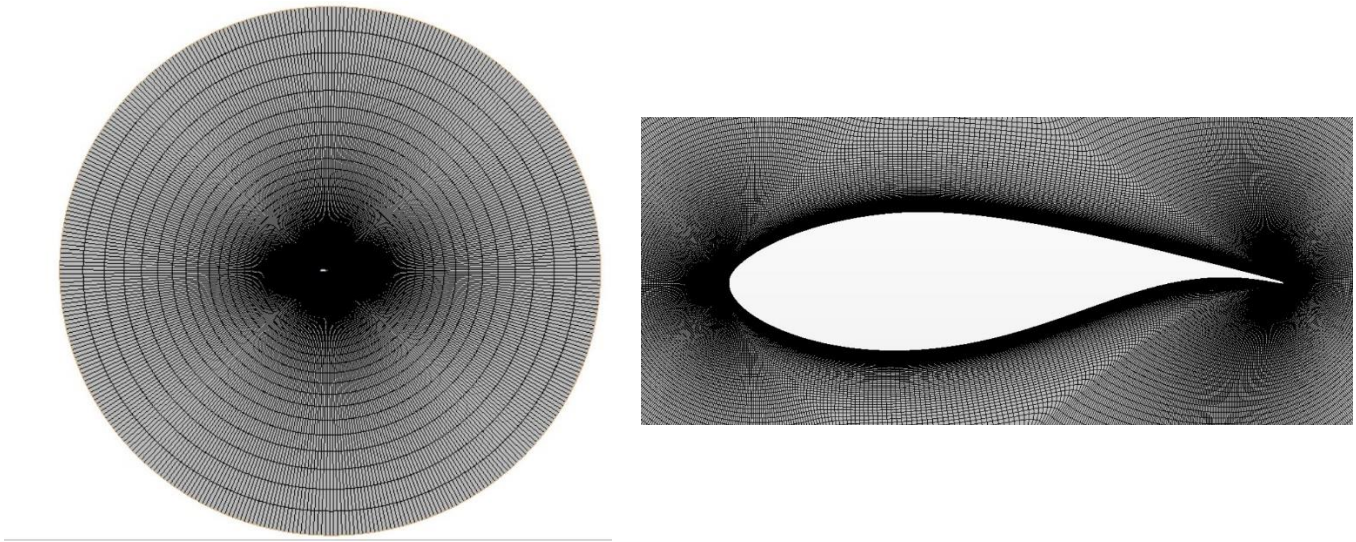

(**a**) (**b**)

Figure 1. Structured mesh generated around the airfoil: (**a**) General view; (**b**) Detailed view.

Two different flow control devices were added to the TE of the airfoil: Gurney flaps and rotating microtabs. A total of 48 different cases with Gurney flaps were considered, with different lengths and angles of attack; and 105 different cases with rotating microtabs, with different lengths (L), orientations (β) and angles of attack. The remaining 5 cases consist of the airfoil without flow control devices. All the studied cases are summarized in Table 1.

Table 1. Analyzed flow control devices and all their configurations.

Flow control device	Length (in % of c)	Orientation	AoA
Clean airfoil	-	-	0°, 2°, 4°, 6°, 9°
Gurney Flap	0.25, 0.5, 0.75, 1, 1.25, 1.5, 1.75, 2	-	0°, 2°, 4°, 6°, 9°
Rotating Microtab	1, 1.5, 2	0°, -15°, -30°, -45°, -60°, -75°, -90°	0°, 1°, 2°, 3°, 4°, 5°

These flow control devices were added to the previously-explained mesh by the cell-set model. This modelling technique consists of defining a geometry on an already-generated mesh, and then, splitting this geometry into a new region, and defining it as wall with no-slip conditions. As demonstrated by Ballesteros-Coll et al. [8], this model is suitable for this kind of problems, since a global relative error of 3.784% of this model in comparison with the fully-resolved model was obtained in that study. Figure 2 illustrates an example of the cell-set model implementation for a rotating microtab.

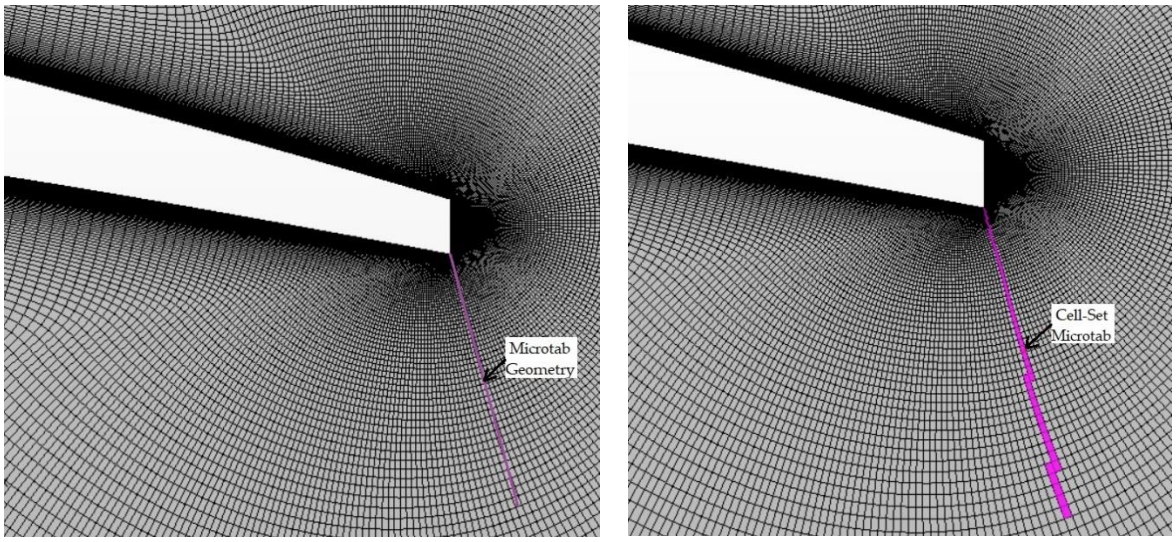

(**a**) (**b**)

Figure 2. Cell-Set implementation for modelling a microtab: (**a**) Geometry of the microtab; (**b**) Microtab generated using the Cell-Set model.

Regarding the fluid physics, the dynamic viscosity of the air was set at $\mu = 1.855 \cdot 10^{-5}$ Pa·s, and the density was set at $\rho = 1.2041$ kg/m^3. The freestream velocity of the flow was set at $U_\infty = 30$ m/s, which means that the Reynolds number (Re) is equal to $2 \cdot 10^6$. For turbulence modelling RANS-based k-ω Shear Stress Transport (SST) model by Menter [25] was chosen, which combines the k-ω model for the near-wall zones and k-ε model for the regions far from the walls.

2.2. Convolutional Neural Network

2.2.1. Input and Output Layers

The domain is represented by four different 128×256 layers. The first two layers represent the geometry of the airfoil and the flow control device, and the other two layers represent the velocity components in both directions.

The layers describing the domain are generated by means of a binary representation, where the points belonging to the geometry are identified with a 1 and those which do not belong to the geometry are identified with a 0. One of these layers provides an overview of the airfoil, while the other provides a close-up view of the airfoil TE, showing the flow control device in detail. Figure 3a shows the zones represented by each layer, and Figure 3b and Figure 3c display and example of these two layers.

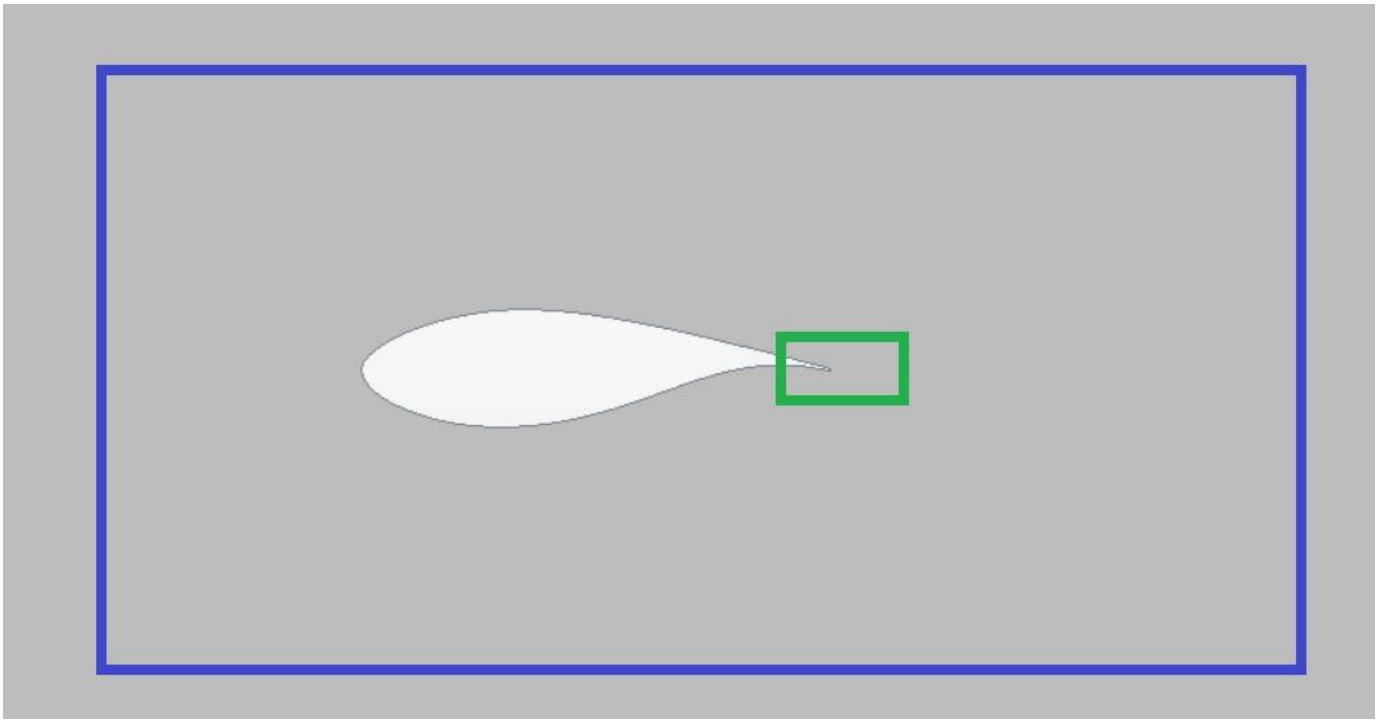

(**a**)

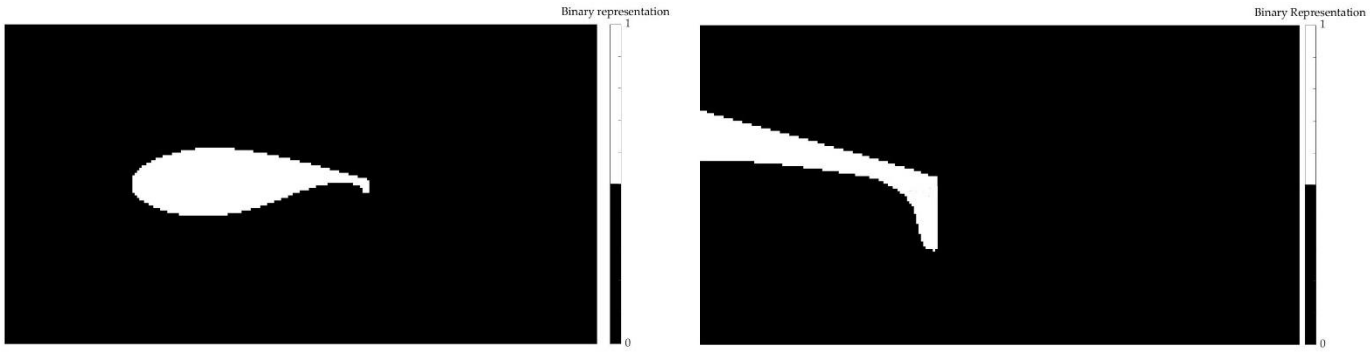

(**b**) (**c**)

Figure 3. Domain representation layers of a Gurney flap: (**a**) Sketch of the area represented by each layer (airfoil overview layer marked in blue and flow control device close-up layer marked in green); (**b**) Airfoil overview layer; (**c**) Close-up view of the flow control device layer.

The velocity layers provide the value of the velocity components. These layers are used to determine the AoA of the airfoil accurately, since in the above-explained binary-representation layers, slight variations in orientation may not be correctly represented. Figure 4a and 4b show the velocity layers, which represent the x and y components of the velocity, respectively.

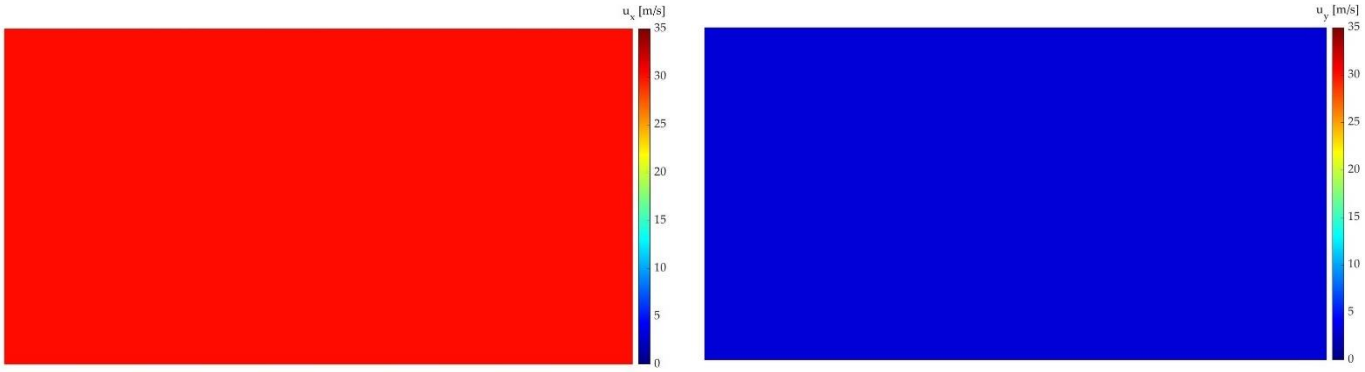

(**a**) (**b**)

Figure 4. Velocity component layers: (**a**) Component in x direction; (**b**) Component in x direction. 144

Concerning the output of the networks, three layers and two scalars are considered. The three layers correspond to the velocity (both components) and pressure fields on the TE of the airfoil, and the scalars are the C_D and C_L coefficients. 145 146 147

To prepare the output layers, the values were first interpolated to fit into a 128×256 arrays. Then, the values of those arrays were normalized, following Expressions (1), (2) and (3). 148 149

$$u_x^* = \frac{u_x}{u_\infty} \quad (1)$$

$$u_y^* = \frac{u_y}{u_\infty} \quad (2)$$

$$p^* = \frac{p}{\rho \cdot u_\infty^2} \quad (3)$$

where u_x^*, u_y^* and p^* are the dimensionless variables. 150

Finally, all the values of the layers are ranged between 0 and 1 following Expression (4), in order to speed up and enhance the training process. 151 152

$$\Phi' = \frac{\Phi - \min(\Phi)}{\max(\Phi) - \min(\Phi)} \quad (4)$$

where Φ is replaced by each dimensionless variable. 153

This last step is also followed to range between 0 and 1 the input layers and the output scalars corresponding to the coefficients. 154 155

2.2.2. CNN Architecture 156

In the present paper, two different CNN are considered, one for velocity and pressure field prediction, and another one for drag and lift coefficient prediction. This networks were designed and trained using MATLAB 2021a [26] commercial code with its Deep Learning Toolbox [27].

For velocity and pressure field prediction, an U-Net architecture [28] is proposed, based on the previous works from Ribeiro et al. [14] and Thuerey et al. [17]. The U-Net architecture is a special case of an encoder-decoder network. The proposed network consists of four encoder/decoder blocks. Each encoder block contains two convolutional layers. The first one is followed by a ReLU (Rectifier Linear Unit) layer, and the second one is followed by a ReLU layer and a Max Pooling layer. The kernel size of the first two encoding blocks is equal to 5, and strided convolutions are performed on those blocks, in order to reduce the data size for the training step. The kernel size of the last blocks is equal to 3. After each encoding block, the number of filters is doubled. The decoding blocks perform the reverse process of their symmetrical blocks of the encoding phase, and they are connected to the encoding blocks by concatenation layers. Figure 5 provides a schematic view of the explained network.

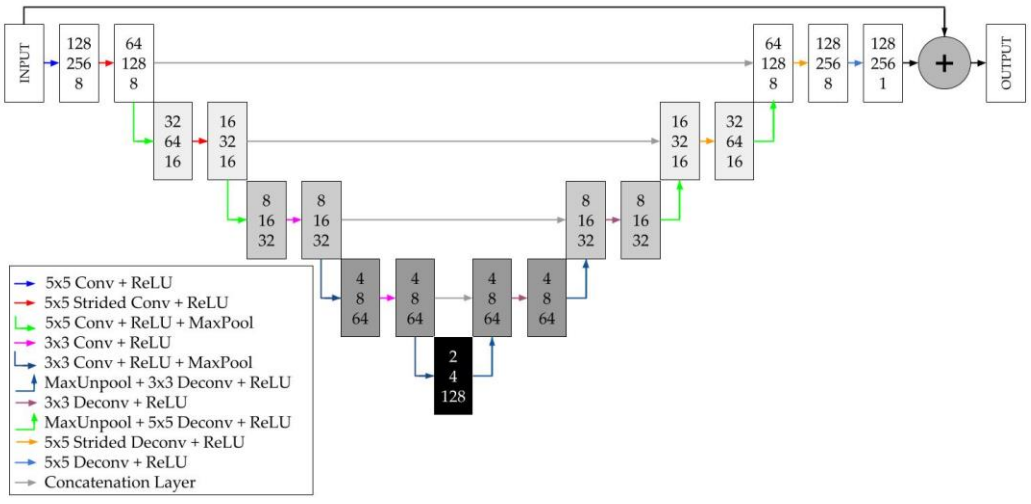

Figure 5. Schematic view of the proposed CNN for velocity and pressure field prediction.

For lift and drag coefficient prediction, only the encoding part of the CNN is considered. In this case, a fully connected layer is added after the last layer. Unlike the complete structure, this

network does not return a layer, it returns two scalar values, C_D and C_L. Figure 6 shows a schematic view of this network.

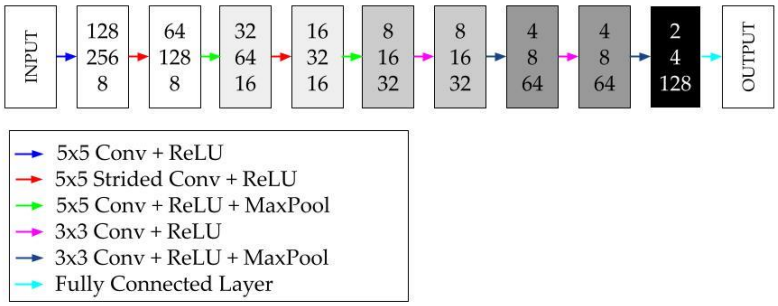

Figure 6. Schematic view of the proposed CNN for aerodynamic coefficient prediction.

For the network training, Adam [29] optimizer is employed in both cases, with a batch size of 64. For field prediction, a learning rate of 0.001 and a weight decay of 0.0005 is selected; and for coefficient prediction a learning rate of 0.0001 and a weight decay of 0.0005. From the dataset of 158 samples, 21 are considered for testing the network. The other 137 are divided into 70% training and 30% validation for field prediction and 90% training and 10% validation for coefficient prediction.

These hyperparameters and data-splitting ratios were selected after training this network with 27 different configurations of these parameters. From the analyzed configurations, the selected ones provide the minimum Root-Mean-Square Error (RMSE) of the analyzed magnitude. Appendix A provides a summary of the considered configurations and the obtained RMSE for each magnitude and coefficient.

3. Results and Discussion

In order to determine the accuracy of the proposed CNN, the predictions of this CNN have been compared with those obtained by CFD. For this comparison, the 21 simulations of the test-set mentioned above are considered.

3.1. Velocity and pressure field prediction

The velocity and pressure fields obtained by the CNN are both qualitatively and quantitatively compared in order to determine the accuracy of the proposed CNN for field prediction. For the

qualitative comparison, four different cases are considered, each one with a different geometry and AoA. All these cases can be found in Figure 7.

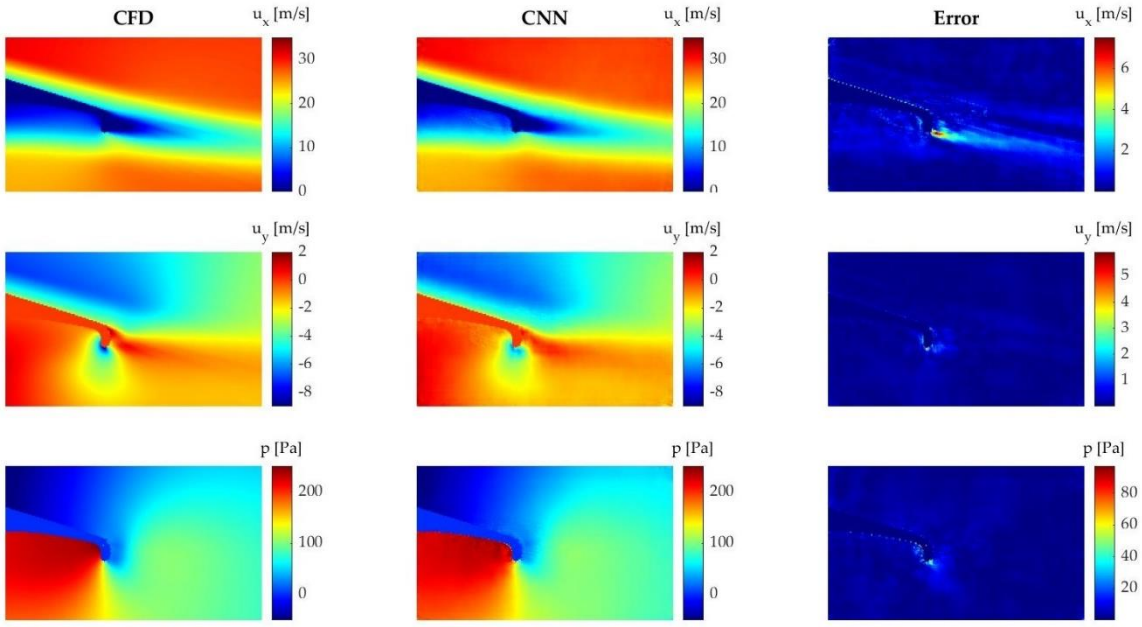

(**a**)

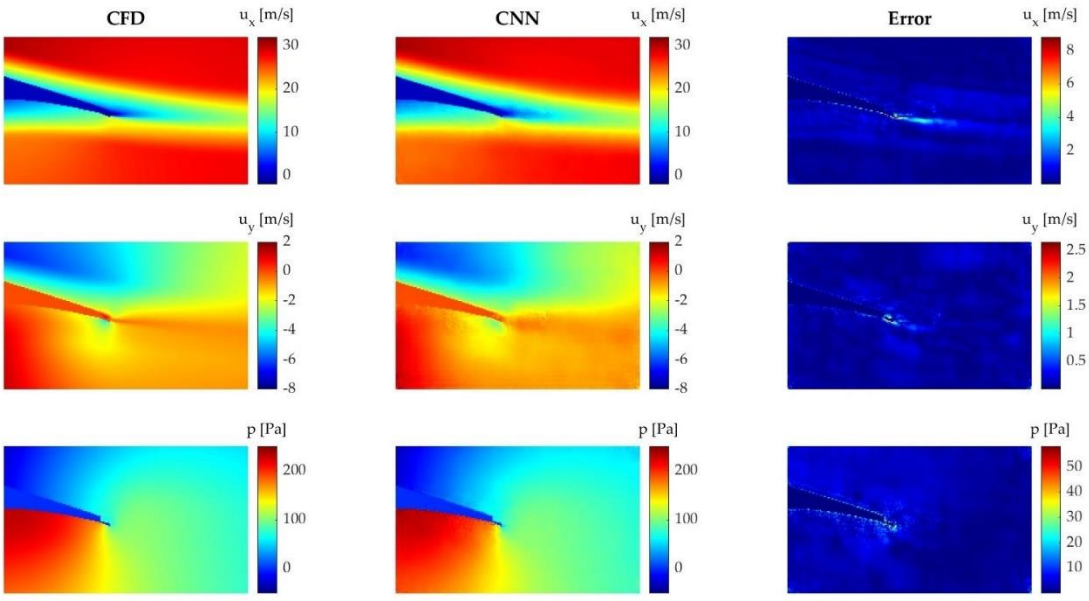

(**b**)

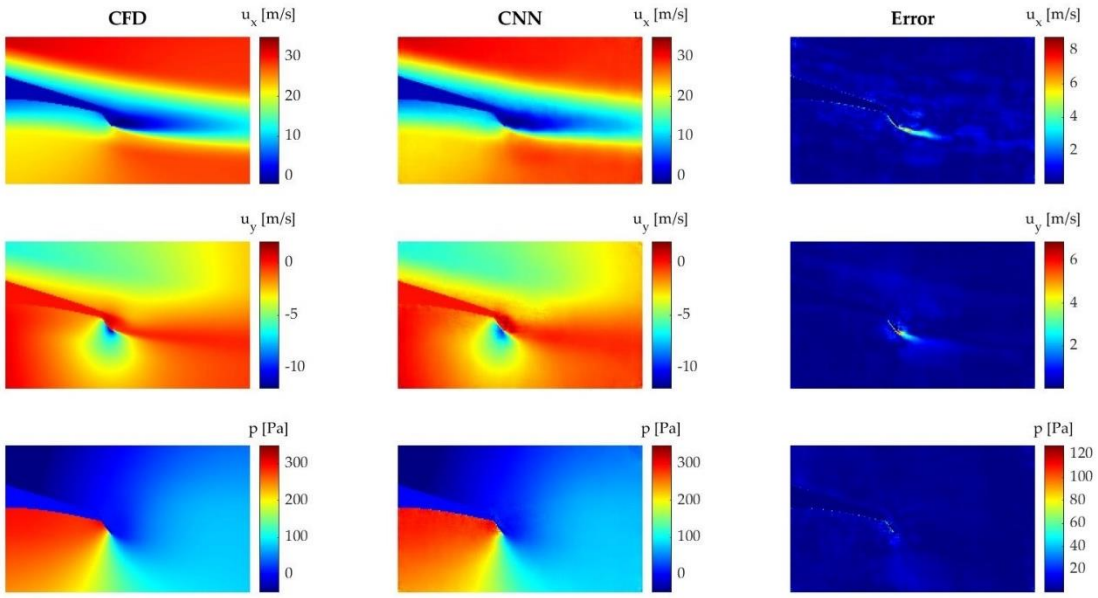

(**c**)

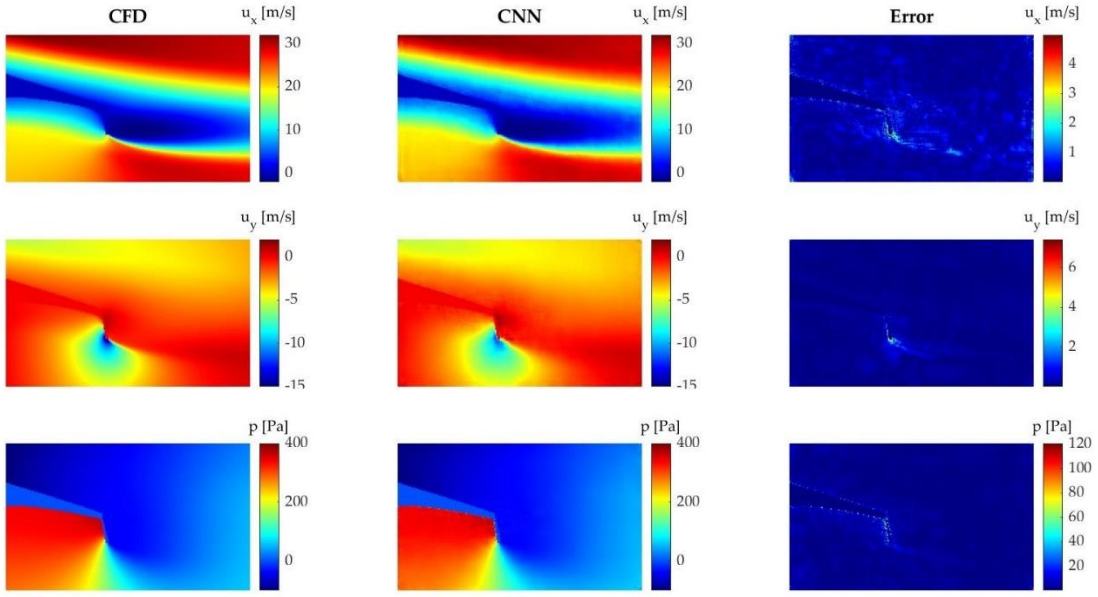

(**d**)

Figure 7. Comparison of the velocity and pressure fields obtained by means of CFD and CNN: (**a**) Gurney flap L=1% and AoA=0°; (**b**) Microtab L=1%, β=-15° and Aoa=2°; (**c**) Microtab L=1.5%, β=-45° and AoA=6°; (**d**) Microtab L=2%, β=-75° and AoA=9°.

The results show that the proposed CNN is able to accurately predict the velocity and pressure fields around the flow control devices in all the tested cases. The most problematic area is the wake behind the flow control device in all the analyzed cases, especially when predicting u_x. Some errors are also visible in the contour of the airfoil. In geometries which have surfaces perpendicular to the

flow, i.e., Gurney flaps and rotating microtabs with high angles of orientation, slight errors of velocity fields appear at the front side of the flow control device. However, the CNN is able to reliably predict the flow characteristics, and all these mentioned errors are not considered significant.

In order to obtain a quantitative view of these results, data distribution histograms are made for each analyzed magnitude. In agreement with the qualitatively compared fields, the data distribution histograms show nearly equal shapes, being the ranges with the most data the only ones where differences between the two methods can be appreciated. Figure 8 shows data distribution histograms.

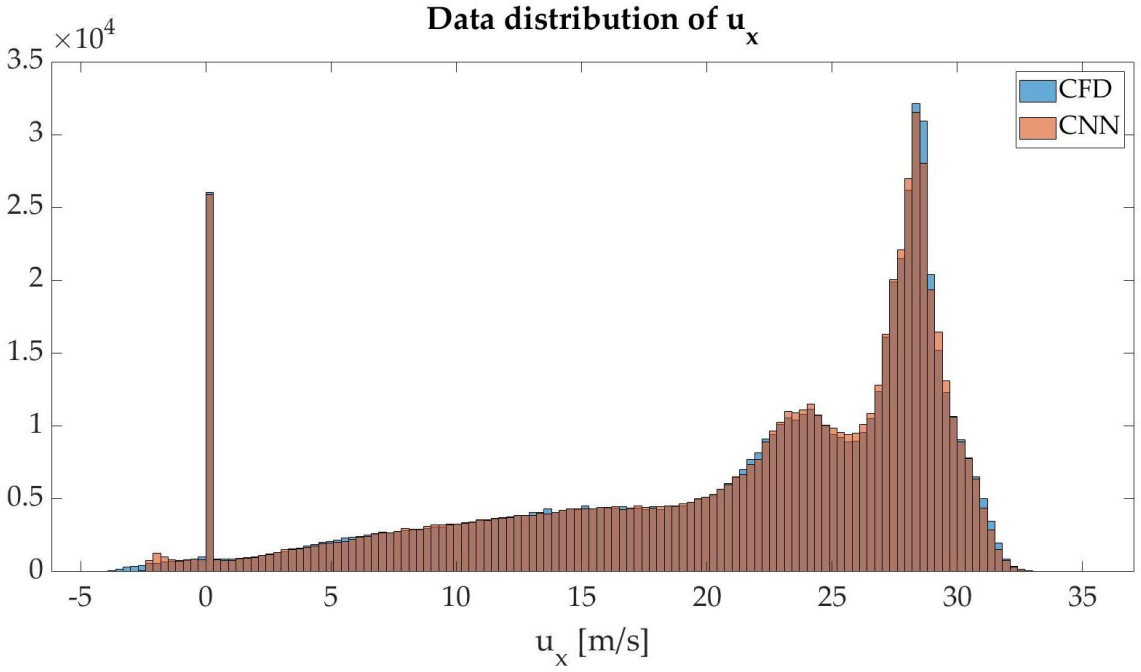

(**a**)

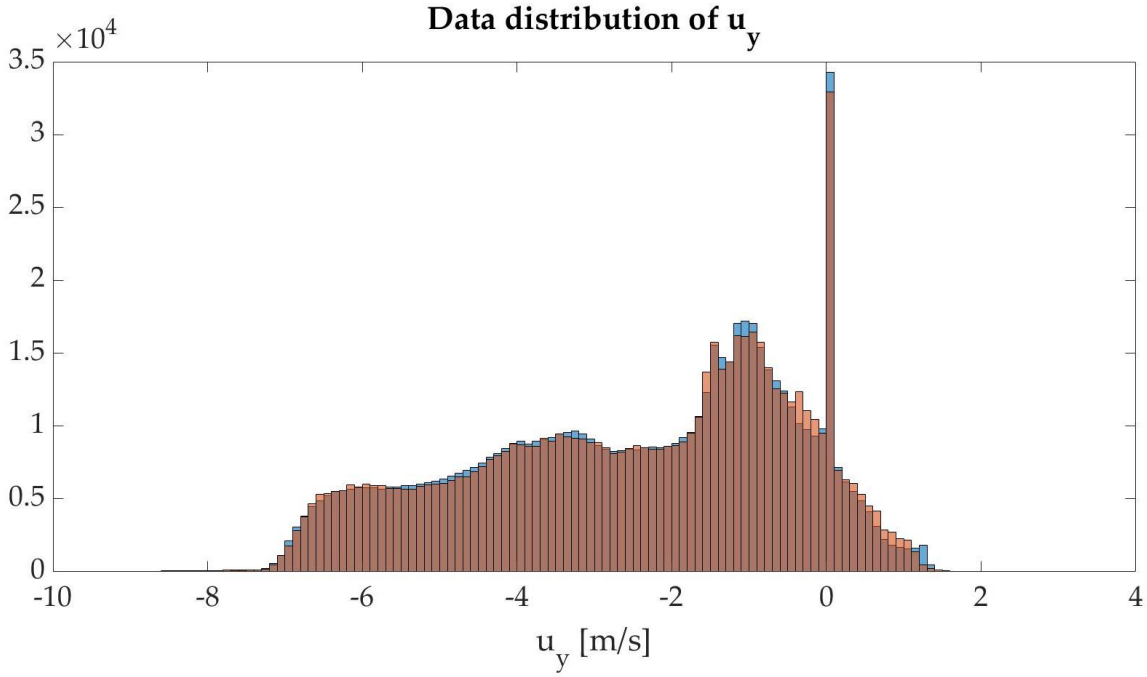

(**b**)

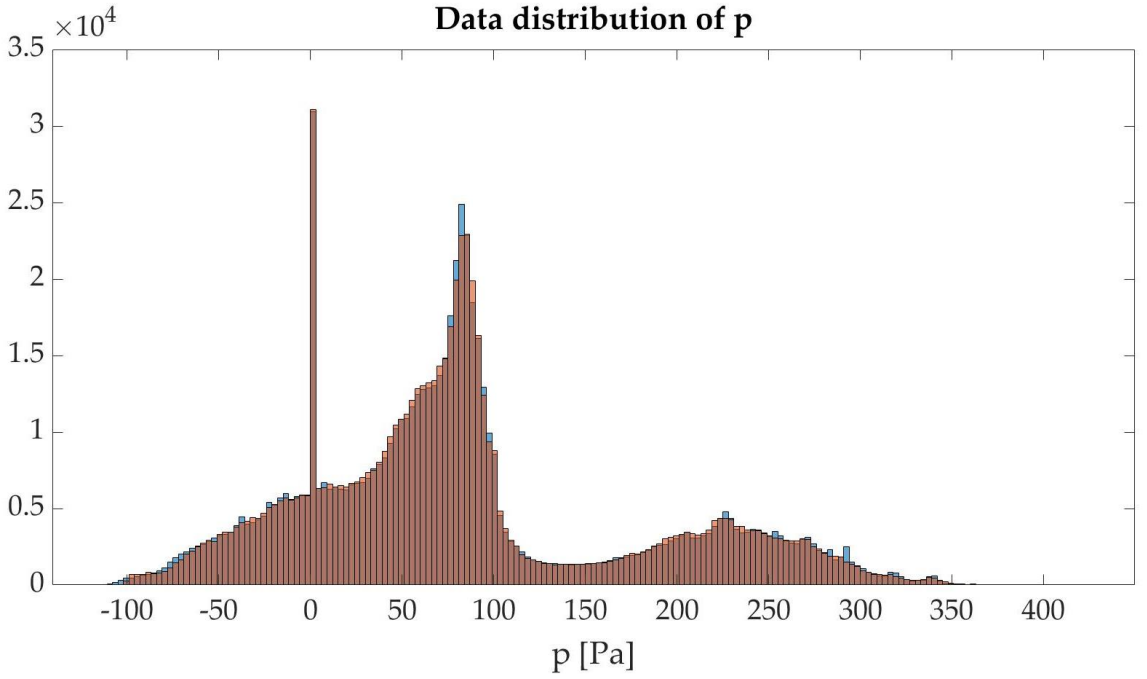

(**c**)

Figure 8. Data distribution histogram of the test-set: (**a**) Data distribution of u_x; (**b**) Data distribution of u_y; (**c**) Data distribution of p.

In addition, the arithmetic mean (μ) and standard deviation (σ) of both methods are calculated from the data distribution histograms. These two values, in accordance with all the results shown above, show almost equal values for all magnitudes, as shown in Table 2.

Table 2. Arithmetic mean and standard deviation of the results obtained by CFD and CNN.

Method	CFD			CNN		
	u_x	u_y	p	u_x	u_y	p
Arithmetic mean (μ)	20.9538	-2.5385	82.8164	20.9784	-2.5076	82.9625
Standard deviation (σ)	8.7620	2.0860	91.6118	8.7086	2.0939	90.7867

3.2. *Aerodynamic coefficient prediction*

In order to evaluate the accuracy of the network for predicting aerodynamic coefficients, the predicted C_D and C_L coefficients are compared to the benchmark values obtained by CFD simulations. In addition, the lift-to-drag (C_L/C_D) coefficient, which is calculated from the predicted coefficients, is also compared. The plots from Figure 9 provide this comparison.

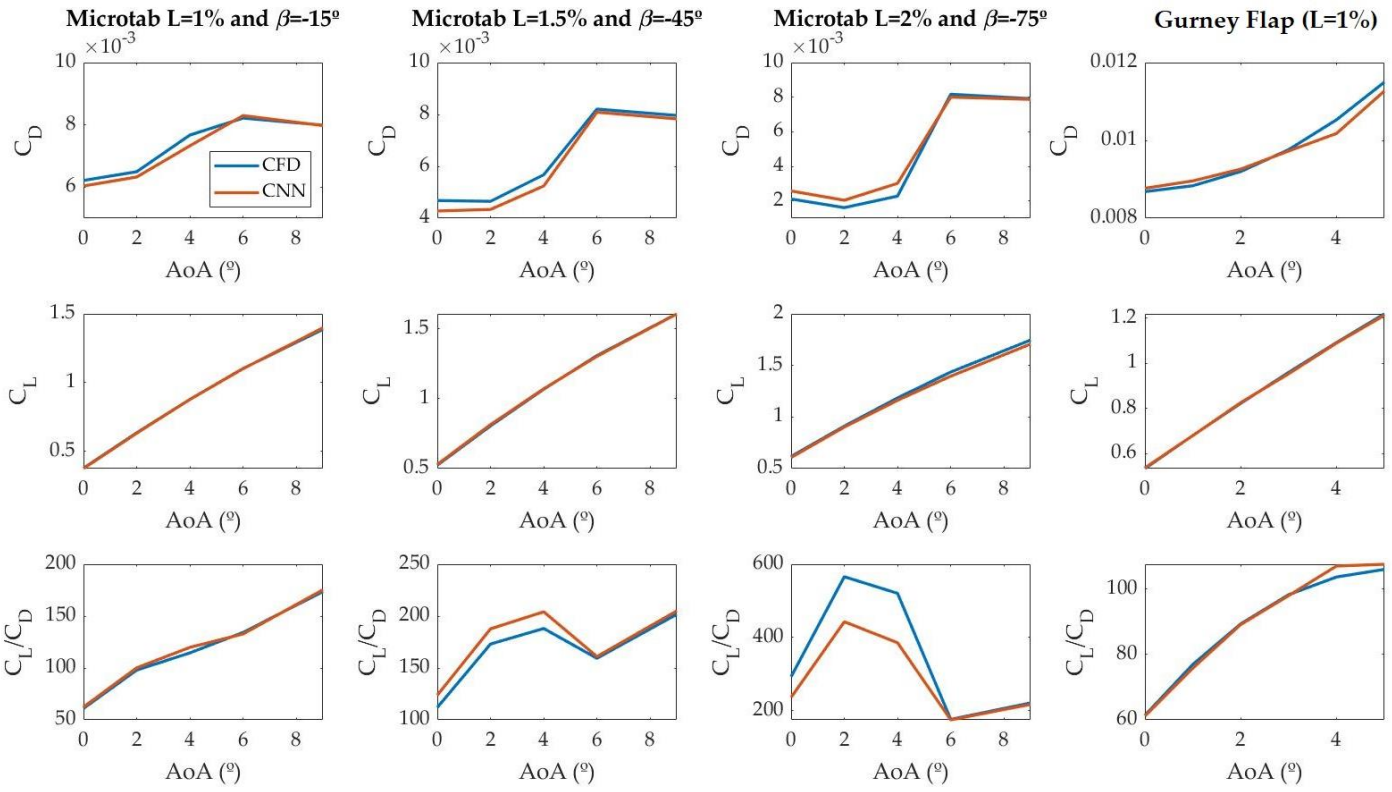

Figure 9. Aerodynamic coefficient comparison of all the tested cases.

As the plots demonstrate, the CNN is able to reliably predict aerodynamic coefficients. In the case of microtabs, C_D values increase exponentially with low AoAs, and subsequently, for AoA>6°,

they decrease slightly. In the case of the Gurney flaps, this upward trend can also be seen throughout the analyzed range. In contrast, C_L values follow a linear trend with respect to AoA in all the cases considered. With microtabs, the C_D/C_L ratio shows a sharp rise for low AoA, followed by a less pronounced drop and a further stabilization for high AoA. The rise and the fall are more pronounced as the length of the microtab increases. When using Gurney flaps the C_D/C_L coefficient follows a logarithmic trend, tending to flatten out for AoA>4°.

C_D predictions show small discrepancies between the two methods. With microtabs these differences become more noticeable as the microtab length increases and the AoA decreases, and with Gurney flaps as the AoA increases. In contrast, the predictions of the C_L are almost the same in all the studied cases. Nevertheless, the results show that the network is able to predict this trend, with values close to those obtained by CFD.

In order to quantify the results, the absolute and relative errors of the predictions are studied. These errors are shown in Table 3. As previously demonstrated, the errors of the C_D predictions are higher than those of C_L, with a maximum relative error of 32.44%. However, the average relative error is 6.17%, which is considered acceptable. Low errors are observed in all the C_L predictions, with an average relative error of 0.827%.

Table 3. Summary of absolute and relative error of C_D and C_L coefficients predicted by the CNN.

Error	C_D			C_L		
	Min	**Max**	**Mean**	**Min**	**Max**	**Mean**
Absolute error	0.00002	0.00074	0.00023	0.0005	0.04	0.0089
Relative error	0.19%	32.44%	6.17%	0.033%	2.786%	0.827%

3.3. *Performance analysis*

The main objective of using neural networks to predict flows is to reduce the computational time required to run CFD simulations. Therefore, the computational time requirements for each method are compared. As shown in Table 4, neural networks clearly outperform CFD simulations in terms of computational time. As expected due to its simplicity, the CNN for aerodynamic coefficient prediction is the fastest one, being 16148 times faster than the CFD simulations. However, the complete CNN used for field prediction is also considerably fast, being 7529 times faster than

the CFD. A single core of an Intel Xeon 5420 CPU was used for running CFD simulations and CNNs.

Table 4. Computational time requirement comparison.

Method	Computational time [s]	Speedup
CFD	53612	-
CNN (Field prediction)	7.12	7529
CNN (Coefficient prediction)	3.32	16148
CNN (Total)	10.44	5135

4. Conclusions

In the present work, two different CNNs are proposed. One of them predicts the velocity and pressure fields around flow control devices implemented in the TE of the DU91W(2)250 airfoil, and the other one predicts the C_D and C_L aerodynamic coefficients of the airfoil for the same cases. These networks were trained and evaluated using the results obtained from CFD simulations, in which the cell-set model was used to implement the flow control devices. The dataset contains a total of 158 cases, with two different flow control devices, rotating microtabs and Gurney flaps, with different geometries and under different conditions.

Regarding the CNN for field prediction, the results indicate that the proposed network is able to predict the main flow characteristics around the flow control device, with very low errors, which mainly appear on the wake behind the flow control device and on the contour of the airfoil. With respect to aerodynamic coefficients, the CNN is also able to predict them accurately, with mean relative errors of 6.17% for C_D and 0.827% for C_L. In both cases, the networks are sensitive to small changes of the geometry or the AoA, which is a key feature for geometry optimization.

In terms of computational time, the proposed networks clearly outperform the CFD simulations, reducing the computational time in four orders of magnitude.

Therefore, this paper demonstrates that flow control devices can be studied by means of neural networks, with acceptable errors and a significative reduction of required computational time and resources.

Author Contributions: Conceptualization, K.P.-P.; methodology, K.P.-P. and A.B.-C.; software, E.Z. and A.Z.; validation, A.B.-C., E.Z. and U.F.-G.; formal analysis, K.P.-P. and A.B.-C.; investigation, K.P.-P. and A.B.-C.; resources, U.F.-G. and E.Z.; data curation, A.Z.; writing—original draft preparation, K.P.-P.; writing—review and editing, K.P.-P. and U.F.-G.; visualization, A.B.-C. and E.Z.; supervision, U.F.-G.; project administration, U.F.-G.; funding acquisition, U.F.-G. All authors have read and agreed to the published version of the manuscript.

Funding: The authors are thankful to the government of the Basque Country for the ELKARTEK21/10 KK-2021/00014 and ITSAS-REM IT1514-22 research programs, respectively

Acknowledgments: The authors are grateful for the support provided by the SGIker of UPV/EHU. This research was developed under the frame of the Joint Research Laboratory on Offshore Renewable Energy (JRL-ORE).

Conflicts of Interest: The authors declare no conflict of interest.

Nomenclature

AI	Artificial Intelligence
ANN	Artificial Neural Network
CFD	Computational Fluid Dynamics
CNN	Convolutional Neural Network
DL	Deep Learning
HAWT	Horizontal Axis Wind Turbine
RANS	Reynolds-Averaged Navier-Stokes
ReLU	Rectifier Linear Unit
RMSE	Root-Mean-Square Error
SST	Shear Stress Transport
TE	Trailing Edge
VG	Vortex Generator
*	Dimensionless variable
‘	Variable ranged between 0 and 1
AoA	Angle of Attack
β	Flow control device orientation
c	Airfoil chord length
C_D	Drag coefficient
C_L	Lift coefficient
C_L/C_D	Lift-to-drag ratio
Δz	First cell height
L	Flow control device length
ρ	Density
R	O-mesh radius
Re	Reynolds number
μ	Dynamic viscosity
U_∞	Freestream velocity

References

1. Barlas, T.K.; van Kuik, G.A.M. Review of State of the Art in Smart Rotor Control Research for Wind Turbines. *Prog. Aerosp. Sci.* **2010**, *46*, 1–27, doi:10.1016/j.paerosci.2009.08.002.
2. Aramendia, I.; Fernandez-Gamiz, U.; Ramos-Hernanz, J.A.; Sancho, J.; Lopez-Guede, J.M.; Zulueta, E. Flow Control Devices for Wind Turbines. In *Energy Harvesting and Energy Efficiency*; Bizon, N., Mahdavi Tabatabaei, N., Blaabjerg, F., Kurt, E., Eds.; Lecture Notes in Energy; Springer International Publishing: Cham, 2017; Vol. 37, pp. 629–655 ISBN 978-3-319-49874-4.
3. Aramendia-Iradi, I.; Fernandez-Gamiz, U.; Sancho-Saiz, J.; Zulueta-Guerrero, E. State of the Art of Active and Passive Flow Control Devices for Wind Turbines. *DYNA* **2016**, *91*, 512–516, doi:http://dx.doi.org/10.6036/7807.
4. Alber, J.; Soto-Valle, R.; Manolesos, M.; Bartholomay, S.; Nayeri, C.N.; Schönlau, M.; Menzel, C.; Paschereit, C.O.; Twele, J.; Fortmann, J. Aerodynamic Effects of Gurney Flaps on the Rotor Blades of a Research Wind Turbine. *Wind Energy Sci.* **2020**, *5*, 1645–1662, doi:10.5194/wes-5-1645-2020.
5. Nakafuji, D.T.Y.; van Dam, C.P.; Smith, R.L.; Collins, S.D. Active Load Control for Airfoils Using Microtabs. *J. Sol. Energy Eng.* **2001**, *123*, 282–289, doi:10.1115/1.1410110.
6. Fernandez-Gamiz, U.; Zulueta, E.; Boyano, A.; Ramos-Hernanz, J.A.; Lopez-Guede, J.M. Microtab Design and Implementation on a 5 MW Wind Turbine. *Appl. Sci.* **2017**, *7*, 536, doi:10.3390/app7060536.
7. Aramendia, I.; Fernandez-Gamiz, U.; Zulueta, E.; Saenz-Aguirre, A.; Teso-Fz-Betoño, D. Parametric Study of a Gurney Flap Implementation in a DU91W(2)250 Airfoil. *Energies* **2019**, *12*, 294, doi:10.3390/en12020294.
8. Ballesteros-Coll, A.; Fernandez-Gamiz, U.; Aramendia, I.; Zulueta, E.; Lopez-Guede, J.M. Computational Methods for Modelling and Optimization of Flow Control Devices. *Energies* **2020**, *13*, 3710, doi:10.3390/en13143710.
9. Ballesteros-Coll, A.; Portal-Porras, K.; Fernandez-Gamiz, U.; Zulueta, E.; Lopez-Guede, J.M. Rotating Microtab Implementation on a DU91W250 Airfoil Based on the Cell-Set Model. *Sustainability* **2021**, *13*, 9114, doi:10.3390/su13169114.
10. Ibarra-Udaeta, I.; Portal-Porras, K.; Ballesteros-Coll, A.; Fernandez-Gamiz, U.; Sancho, J. Accuracy of the Cell-Set Model on a Single Vane-Type Vortex Generator in Negligible Streamwise Pressure Gradient Flow with RANS and LES. *J. Mar. Sci. Eng.* **2020**, *8*, 982, doi:10.3390/jmse8120982.
11. Portal-Porras, K.; Fernandez-Gamiz, U.; Aramendia, I.; Teso-Fz-Betoño, D.; Zulueta, E. Testing the Accuracy of the Cell-Set Model Applied on Vane-Type Sub-Boundary Layer Vortex Generators. *Processes* **2021**, *9*, 503, doi:10.3390/pr9030503.
12. Ye, S.; Zhang, Z.; Song, X.; Wang, Y.; Chen, Y.; Huang, C. A Flow Feature Detection Method for Modeling Pressure Distribution around a Cylinder in Non-Uniform Flows by Using a Convolutional Neural Network. *Sci. Rep.* **2020**, *10*, 4459, doi:10.1038/s41598-020-61450-z.
13. Guo, X.; Li, W.; Iorio, F. Convolutional Neural Networks for Steady Flow Approximation. In Proceedings of the Proceedings of the 22nd ACM SIGKDD International Conference on Knowledge Discovery and Data Mining; ACM: San Francisco California USA, August 13 2016; pp. 481–490.
14. Ribeiro, M.D.; Rehman, A.; Ahmed, S.; Dengel, A. DeepCFD: Efficient Steady-State Laminar Flow Approximation with Deep Convolutional Neural Networks. *ArXiv200408826 Phys.* **2020**.
15. Portal-Porras, K.; Fernandez-Gamiz, U.; Ugarte-Anero, A.; Zulueta, E.; Zulueta, A. Alternative Artificial Neural Network Structures for Turbulent Flow Velocity Field Prediction. *Mathematics* **2021**, *9*, 1939, doi:10.3390/math9161939.
16. Abucide-Armas, A.; Portal-Porras, K.; Fernandez-Gamiz, U.; Zulueta, E.; Teso-Fz-Betoño, A. A Data Augmentation-Based Technique for Deep Learning Applied to CFD Simulations. *Mathematics* **2021**, *9*, 1843, doi:10.3390/math9161843.
17. Thuerey, N.; Weißenow, K.; Prantl, L.; Hu, X. Deep Learning Methods for Reynolds-Averaged Navier–Stokes Simulations of Airfoil Flows. *AIAA J.* **2020**, *58*, 25–36, doi:10.2514/1.J058291.
18. Spalart, P.; Allmaras, S. A One-Equation Turbulence Model for Aerodynamic Flows. In Proceedings of the 30th Aerospace Sciences Meeting and Exhibit; American Institute of Aeronautics and Astronautics: Reno, NV, U.S.A., January 6 1992.

19. Bhatnagar, S.; Afshar, Y.; Pan, S.; Duraisamy, K.; Kaushik, S. Prediction of Aerodynamic Flow Fields Using Convolutional Neural Networks. *Comput. Mech.* **2019**, *64*, 525–545, doi:10.1007/s00466-019-01740-0.
20. Chen, H.; He, L.; Qian, W.; Wang, S. Multiple Aerodynamic Coefficient Prediction of Airfoils Using a Convolutional Neural Network. *Symmetry* **2020**, *12*, 544, doi:10.3390/sym12040544.
21. Rodriguez-Eguia, I.; Errasti, I.; Fernandez-Gamiz, U.; Blanco, J.M.; Zulueta, E.; Saenz-Aguirre, A. A Parametric Study of Trailing Edge Flap Implementation on Three Different Airfoils Through an Artificial Neuronal Network. *Symmetry* **2020**, *12*, 828, doi:10.3390/sym12050828.
22. Jonkman, J.; Butterfield, S.; Musial, W.; Scott, G. *Definition of a 5-MW Reference Wind Turbine for Offshore System Development*; 2009; p. NREL/TP-500-38060, 947422;
23. STAR-CCM+ V2019.1 Available online: https://www.plm.automation.siemens.com/ (accessed on 2 June 2020).
24. Sørensen, N.N.; Méndez, B.; Muñoz, A.; Sieros, G.; Jost, E.; Lutz, T.; Papadakis, G.; Voutsinas, S.; Barakos, G.N.; Colonia, S.; et al. CFD Code Comparison for 2D Airfoil Flows. *J. Phys. Conf. Ser.* **2016**, *753*, 082019, doi:10.1088/1742-6596/753/8/082019.
25. Menter, F.R. Two-Equation Eddy-Viscosity Turbulence Models for Engineering Applications. *AIAA J.* **1994**, *32*, 1598–1605, doi:10.2514/3.12149.
26. MATLAB Available online: https://es.mathworks.com/products/matlab.html (accessed on 9 June 2021).
27. Deep Learning Toolbox Available online: https://es.mathworks.com/products/deep-learning.html (accessed on 3 July 2021).
28. Ronneberger, O.; Fischer, P.; Brox, T. U-Net: Convolutional Networks for Biomedical Image Segmentation. In Proceedings of the Medical Image Computing and Computer-Assisted Intervention – MICCAI 2015; Navab, N., Hornegger, J., Wells, W.M., Frangi, A.F., Eds.; Springer International Publishing: Cham, 2015; pp. 234–241.
29. Kingma, D.P.; Ba, J. Adam: A Method for Stochastic Optimization. *ArXiv14126980 Cs* **2017**.

Supplementary Files

This is a list of supplementary files associated with this preprint. Click to download.

- Supplementary.docx